Research Article

Impact of Uniaxial Mechanical Perturbation on Structural Properties and Smectite Porosity Features: Ion Exchanger Efficiency and Adsorption Performance Fate

Walid Oueslati [ID], Chadha Mejri, and Abdesslem Ben Haj Amara

Université de Carthage, Faculté des Sciences de Bizerte, LR19ES20, Ressources, Matériaux et Ecosystèmes (RME), Bizerte 7021, Tunisia

Correspondence should be addressed to Walid Oueslati; walidoueslati@ymail.com

The use of montmorillonite in the context of engineered barriers makes it possible to minimize the spread of heavy metals from industrial and even radioactive waste. An evaluation of the performance of the mechanisms controlling the clay-environment interaction and predicting the dynamics/configuration of the interlayer space (IS) is required. This work focuses on a quantitative identification of the structural changes and porosity alteration in the case of heavy metal-exchanged montmorillonite samples (Co^{2+} and Cd^{2+} cations) undergoing mechanical stresses (uniaxial oedometric test (loading/unloading)). Relationships between mechanical stress strength, intrinsic structural response, ion exchanger efficiency, and adsorption performance fate are investigated. This goal is achieved through the correlation of in situ quantitative X-ray diffraction (XRD) analysis (under an extremely controlled atmosphere reached by varying relative humidity rate %rh) and porosity investigation (assured by combining outcomes from BET (Brunauer–Emmett–Teller) and BJH- (Barrett, Joyner, and Halenda-) PSD (pore size distribution) analysis). Obtained results show an upsurge in the structural heterogeneities accompanying the theoretical increase in the mixed layer structure (MLS) number and developing an unconventional hydration behaviour after stress relaxation regardless of exchangeable cation nature. Experimental XRD patterns are reproduced using MLS, which suggests the coexistence of more than one "crystallite" specie and more than one exchangeable cation indicating a complex cation exchange capacity (CEC) saturation. For extremely low %rh value, a new homogeneous dehydrated state trend is observed in the case of the Co^{2+} cation. Porosity analysis shows mesopore volume growth for the stressed sample and confirms crystallite exfoliation layer trends, results of the layer cohesion damage, and subsequent constraint strength fluctuations.

1. Introduction

Waste disposal has become one of the most serious modern environmental problems associated with the development of countries. The architecture, design, and operation of the waste disposal sites ensure adequate waste management with respect for human health and the ecosystem. The geological disposal, adopted as a safe solution for the long-term management of radioactive waste, is delivered by a system that (1) isolates waste from the biosphere for extremely prolonged periods of time, (2) ensures that residual radioactive substances reaching the biosphere will be at comparatively insignificant concentrations, and (3) provides reasonable assurance that any risk of inadvertent human intrusion would be extremely low [1–5]. The most common problems of the landfill site are environmental degradation and groundwater contamination [6].

The use of compacted clays, as part of the multibarrier concept, ensures the previously cited requirements [7, 8]. Indeed, the most used materials in landfill disposal are compacted clay liner (CCL) and geosynthetic clay liner (GCL). The main reason for using such materials is their intrinsic properties, such as the large specific surface areas (SSA), the low permeability, the cation exchange capacity (CEC), the high adsorption ability, and the low hydraulic conductivity [6–11]. Compacted clay liners are less

expensive, and it has good attenuation capacity. Clay membranes can be used as toxic gases (originating from the landfill site) eliminator and as a trap for radionuclide migration/diffusion (resulting from a pipeline leak or damage due to various types of stress affecting installation) [12–15]. The clay mineral membranes are exposed to various chemical, biological, and physical stresses, and they are influenced by the subsequent leachate [16–21]. To evaluate the consistency of these membranes, it is important to examine their chemical compatibility with the different fluids or the leachate to which they are subjected [22]. Based on the fine particle size, the homogeneous micropores and the high surface charges, the low hydraulic conductivity, the high adsorption capacity, and the low cost compared with geosynthetic clay (GC), natural bentonites are most prized in this context [23–29]. Indeed, [30] studied the shear strength of compacted clays as affected by the mineral content and wet-dry cycles and demonstrated that the cohesion and frictional strength properties were determined and linked to the proportion of clay minerals and the number of wetting and drying cycles. On the other hand, [31] demonstrated, in the case of compacted clays mixed with a wide range of bentonite for engineered barriers, that compressibility was affected by the bentonite content on geotechnical characteristics.

The use of bentonite, especially as a buffer in the excavated escape galleries between the waste containers and the tunnel walls, achieves important strategic outcomes. Bentonite membrane is usually affected by the surrounding temperature/humidity gradient fluctuation [32, 33]. However, compacted clays present problems with cracking and/or desiccation, especially those containing an appreciable amount of bentonite [34–36]. Numerous studies have shown that compacted clays undergo large physicochemical properties modifications when exposed to a cycle of swelling and/or desiccation-wetting, which constitutes a surrounding variable environmental constraint [28–39]. Montmorillonite fraction, which is a dioctahedral species of the smectite mineral group, can constitute up to 95% of bentonite. These functional materials provide restriction of groundwater access to radioactive waste, promote conditions for mass transfer between waste and groundwater by diffusion, overwhelm the migration of radionuclides in colloidal form into groundwater, ensure effective sorption after possible depressurization of radioactive waste containers, and so on [40–45]. In addition to their presence in the formations housing the storage facilities and their use as backfill material or as sealing material to isolate parts of disposal facility, montmorillonite is also present as a buffer material in the empty space between the package and the host rock [46–48]. The montmorillonite layer structure is constituted by the stacking of two types of sheet: an octahedral sheet O ($MO_4(OH)_2$ with M is a metal cation (Al, Mg)) sandwiched between two tetrahedral sheet T (SiO_4) often labelled T-O-T with an average layer thickness around 10 Å. The layer charge is related to existing isomorphic substitutions in the tetrahedral sheet (Al^{3+}, Si^{4+}) and/or octahedral ones (Mg^{2+}/Li^+, Al^{3+}/Mg^{2+}). This charge deficit is compensated by exchangeable cations (Exc.Cat), coming from the soil solution and incorporated in IS. The presence of solvent (water molecule) facilitates exchangeable cations insertion and enables, respectively, layer thickness expansion, mineral dispersion (colloidal properties) in the soil solution, and micro/macroscopic clay swelling. The progressive layer thickness expansion of the basal spacing value d (001) is done by discrete hydration state going from the dehydrated state (0 W, $d_{001} \approx 10$ Å) to the strongly hydrated ones (4 W, $d_{001} \approx 21$ Å) passing, respectively, by 1 W ($d_{001} \approx 12.4$ Å), 2 W ($d_{001} \approx 15.4$ Å), and 3 W ($d_{001} \approx 18.2$ Å) hydration state [49–54].
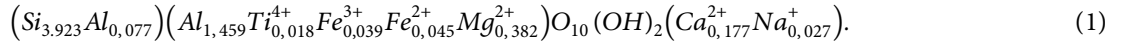
Montmorillonite fraction interacts physically and chemically with soil and the disposal packages over time, which results in structural changes and alteration of the intrinsic properties [48–60]. Depending on these operating constraints (aggressive variable environment), a thorough predictive study of the behaviour and montmorillonite structural response is required. This response can vary from significant structure transformation and properties to yield affected by the nature of the stress.

The applied constraints (aggressive environment) can be considered individually. In this case, they are divided into three groups: (i) atmospheric (temperature, relative humidity, and pressure) and hydrogeological (soil desiccation/wetting cycles) constraints; (ii) chemical constraints (soil solution composition, water chemistry, and soil solution pH); (iii) mechanical stresses (phenomena of sliding/shearing of soils, tectonics and fracturing, and natural mechanical field) [50–53]. In reality, these constraints are often coupled with combinations up to the third coupling order inducing an enormous disruptive stress potential, which affect necessarily the clay fraction efficiency. The performances of the starting materials, according to the initial objectives, are no longer guaranteed; the main problem in this case becomes the effectiveness of these stressed/disturbed materials.

In this work, structural changes, hydration behaviour evolution, CEC alteration, and porosity fate of dioctahedral smectite (Wyoming montmorillonite) subsequent to the applied mechanical stress (uniaxial load/unload) are explored. An experimental investigation protocol, developed at the laboratory scale, based on three main levels is realized. Indeed, mechanical stress based on the loading/unloading test is done to create material stress. An in situ XRD study, under an extremely controlled atmosphere (variable %rh), is directed. The strength of this structural analysis lies in the use of the theoretical 00l diffraction profiles modelling approach to define the relationship between mechanical constraint and microstructure changes. Finally, the adsorption measurement and the PSD analysis are done by targeting the stress damage to the metal-exchanged montmorillonite porosity features.

2. Materials and Methods

2.1. Baseline Sample. Starting sample is a reference montmorillonite specimen (Swy-2) supplied by the Source Clays Repository of the Clay Minerals Society. The intrinsic characteristic properties of this reference sample can be consulted in the literature data [61, 62]. The structural formula per half unit cell is given by [62]

$$\left(Si_{3.923}Al_{0,077}\right)\left(Al_{1,459}Ti_{0,018}^{4+}Fe_{0,039}^{3+}Fe_{0,045}^{2+}Mg_{0,382}^{2+}\right)O_{10}\left(OH\right)_2\left(Ca_{0,177}^{2+}Na_{0,027}^+\right). \quad (1)$$

2.2. Experimental

2.2.1. Na-Rich Montmorillonite.
Raw material requires NaCl pretreatment before application to ensure maximum layer dispersion. This specific treatment is carried out by respecting a classical protocol detailed by [60, 63] to prepare the Na-rich montmorillonite suspension. Indeed, the $<2\,\mu m$ fraction of Wyoming montmorillonite was extracted by allowing larger particles to settle in water and then decanting. The Na-rich montmorillonite was prepared by equilibrating the colloidal fraction with NaCl solution. This step consists of dispersing 40 g of solid in 500 mL of NaCl solution (1 M) and stirring mechanically for 24 h. A SIGMA laboratory centrifuge at 8000 rpm speed is used for the solid fraction separation. To ensure saturation of all exchangeable sites by Na^+ cations, this equilibration was repeated five times. The clay was then washed with distilled water and separated in a high-speed centrifuge until the solution was free of Cl^-. Chloride was presumed to be absent when the supernatant liquid gave a negative test with $AgNO_3$.

2.2.2. Metal-Exchanged Montmorillonite.
The same ionic exchange procedure (used in the case of Na^+ cation) was followed to prepare, respectively, Co-montmorillonite (SWy-Co) and Cd-montmorillonite (SWy-Cd) suspension. This goal is realized using metal chloride solution (1 M) and Na-rich montmorillonite respecting the following chemical reaction:

$$\mathbf{SWy - Na_x + M^{2+} + xCl^- \longrightarrow SWy - M^{2+} + xNaCl,} \quad (2)$$
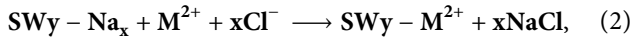
where M^{2+} denotes Co^{2+} and Cd^{2+} cations and SWy-M^{2+} denotes SWy-Co and SWy-Cd.

2.2.3. Experiments.
Before beginning the study of the compaction/reswelling cycle effect on the stressed samples, a study of the unstressed samples under the same controlled atmosphere is essential. The detailed experimental protocol is summarized in Figure 1.

2.3. Mechanical Tests: Materials Fatigue.
The oedometer testing device used is a front-loading oedometer (WF 24251) (Figure 2). The cell diameter is 50 mm. The comparator race extends 12 mm with an accuracy of 2 microns. A predetermined piston pressure can be applied to the metal-exchanged montmorillonite sample, causing fluid expulsion through the filter until the system reaches equilibrium. The Linear Voltage Displacement Transducer (LVDT) measures the displacement of the piston and records the change in the system volume during the test. The measured equilibrium displacement permits the determination of the equilibrium void ratio e, which is defined as the ratio of the fluid volume to that of solid particles. The sample was maintained in contact with an external reservoir of deionized water until the experiment ended. All pressures quoted are gauges; that is, they are pressures relative to atmosphere and hence correspond to the differential pressures causing filtration. Each test consisted of a step-by-step loading and unloading (compaction and swelling) of the clay suspensions. The pressure sequences were 5, 10, 15, 20, 25, and 30 bar for the clay suspension, the same pressures being used during compaction and swelling. At the end of each test, the pressure was totally released, and the sample allowed swelling until equilibrium was reached [64, 65]. Then, the final void ratio e was measured by drying the cake at 140~ overnight. From the known weight of clay fraction M (the amount of suspension introduced in the cell was carefully measured) and the measured piston displacements Δl, the equilibrium void ratio at each pressure can be calculated from the equation

$$e\left(P\right) = e_f + \frac{\Delta l\rho_c A}{M}. \quad (3)$$

In this equation, the Δl values are taken relative to the final position of the piston and may be positive or negative. The dry clay density ρ_c was taken as 2.75 g/cm³ as previously calculated. In both pieces of apparatus, the sample cell is of cross-sectional area $A = 5.07$ cm².

2.4. Structural Analysis.
Experimental XRD patterns are obtained from a Brucker D8 Advance X-ray diffractometer with the following setting and scanning parameters: (i) 40 kV and 20 mA; (ii) Cu_Kα monochromatic radiation $\lambda = 0.15406$ nm; (iii) 0.04°2θ as step size; (iv) angular range 3, 5–60°2θ; (v) 6 s as counting time per step. Diffractometer installation is equipped with an advanced Ansyco humidity (rh) generator connected to a CHC + Cryo & Humidity Anton Paar Chamber. To decode the structural impact of the applied mechanical constraint on the possible deformations affecting the IS configuration, a study of unstressed and stressed samples under extreme values of %rh is carried out. This appeal targets the understanding of the interstitial water retention and release mechanisms. The environmental rh variation extends from 3% to 97%. The desired rh rates are maintained by equilibrating samples for 0.5 hours with their environment.

2.5. Qualitative XRD Analysis.
The qualitative XRD analysis is achieved by QualX 2.0 program [66]. The commercial PDF-2 database associated with the new freely available database POW_COD is used. This analysis targets to identify all present sample phases and provide information, respectively, about the layer thickness (hydrous indication), the 00l reflections positions, and the diffracted profile geometry (based on the symmetry and/or asymmetry peak observations). Additionally, the
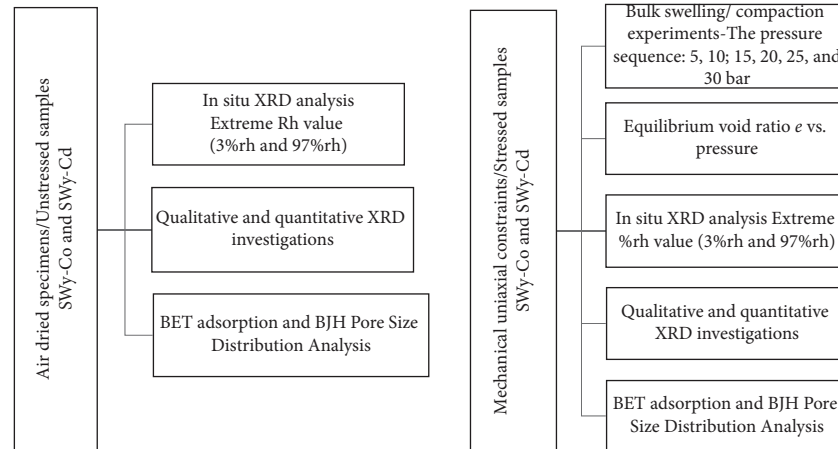
FIGURE 1: Experimental process of the mechanical constraint details, the in situ XRD analysis, and the porosity characterization.
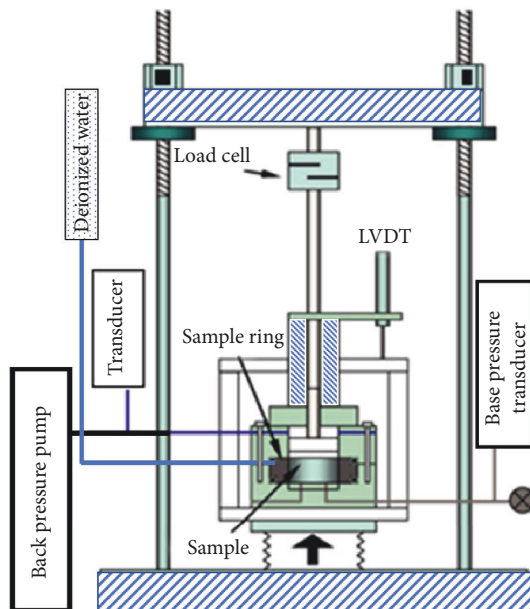

FIGURE 2: Schematic of oedometer installation used for the bulk swelling/compaction experiments.

calculation of "Full Width at Half Maximum" (FWHM) and the rationality deviation parameters (ξ) related to the 00l reflection (calculated as the standard deviation of the $? \times ?_{001}$ values for all $?_i$ measurable reflections over the explored $2\theta°$ angular range) can provide information on the degree of hydration heterogeneity [66–70]. However, the qualitative interpretation of the XRD profile cannot provide a detailed insight into the coexistence of the different phases with their associated relative proportions as well as their different hydration states, which may coexist in the structure. On the other hand, it does not make it possible to follow the evolution and/or the fluctuations of certain structural parameters along the c^* axis. For these reasons, it is necessary to introduce the quantitative XRD analysis based on the XRD modelling approach.

2.6. Modelling (00l) Reflection Profiles.

The theoretical diffracted XRD intensity by a disordered lamellar structure is based on the Drits and Tchoubar [71] algorithm. Based on the expression of the diffracted theoretical intensity, detailed information going from the crystallite size to the elementary tetrahedral or octahedral sheet and its composition can be reached [71]. By optimizing several structural parameters (i.e., Z coordinates of the IS, exchangeable cation position and abundance, and water molecule distribution) during the modelling process, the agreement quality is improved [72–74]. R_{wp} is used as a confidence factor to control this quality [74]. The existing mathematical arsenal behind the modelling approach as well as the details of the fit strategy adopted is exposed in several earlier works [75–77]. It remains to be noted that (per half unit cell) the IS exchangeable cation position respects the provided literature data on similar samples [78, 79].

2.7. Layers Interstratification: Probabilistic Description.

The layers stacking within crystallite is defined by the probabilities of succession of the different layer type, which is described according to the Markovian statistics model. The probability of the presence of one layer is only dependent on the types of layers that precede it. The relationship between the presence of a layer and the preceding types of layers corresponds to the degree of order of the interlayer or Reichweite (R). In soils, the most common Reichweite is $R0$ and $R1$; there are also interstratified $R2$ or $R3$ whose probability of occurrence of a layer depends on the two or three previous layers; the latter are not described in the soils but in the diagenetic series. Equations have been developed [70, 78, 79] to respond to clay interstratification problems. We thus find the probabilistic model where we represent (in a simple case) the stacking of two types of layers A and B of proportions W_A and W_B with the probabilities that layer A follows layer B (P_{BA}). The fundamental equations governing this interstratification are as follows:

$$W_A + W_B = 1 \, P_{AA} + P_{AB} = 1$$
$$P_{BA} + P_{BB} = 1 \, P W_A P_{AB} = W_B P_{BA} \tag{4}$$

Using a combination of the equation, three essential limits for the layers stacking mode appear:

(i) The random stacking $R0$ with $P_{AA} = W_A$ (i.e., no stacking sequence is forbidden; the probability of appearance of a layer in a sequence does not depend on its abundance).

(ii) Stacking with maximum order R1-MPDO prohibiting the succession of two layers in the minority.

(iii) In the case where it is forbidden for two layers of different nature to follow one another ($P_{AB} = P_{BA} = 0$), the probability that two layers of the same nature do so is therefore equal to 1 ($P_{AA} = P_{BB} = 1$), and it is no longer interstratification question but of a physical mixture or total segregation.

It should be noted that the montmorillonite hydration heterogeneities can be treated as layer interstratifications at different hydration states within a clay particle depending on the relative humidity. This can constitute the intermediate hydration state (i.e., 0 W/1 W, 1 W/2 W, and 0 W/1 W/2 W). Hydration heterogeneity is linked to the presence of layer structure heterogeneity (proportion and charge localization of charges) [70, 78, 79].

2.8. Adsorption Measurement and Porosity Investigation. The relationship between mechanical stress and montmorillonite water content affects many geotechnical properties of unsaturated soils, including permeability, volume change, deformation, and shear strength. The main clay properties are mainly controlled by their internal and external surface [80, 81]. The investigation of montmorillonite porosity fate, having undergone structural transformations following the application of mechanical stress, seems essential to confirm quantitative XRD results. Also, the water retention properties are related to the pore structure and the level of external relative humidity experienced. With compaction/reswelling cycles and in situ study by variation of %rh, more layers of water molecules can either be absorbed on the surface of the pores or evacuated by drainage/diffusion by a new transport mechanism.

Adsorption-desorption nitrogen by porous media mainly targets the determination of the surface area (SA) and the pore size distribution (PSD). Montmorillonite powders are obtained by drying each sample. The porosity characteristics are entirely determined by nitrogen sorption [82]. The adsorbed gas amount gives a complete description of the porosity state and even the overall structure [82–86]. Quantachrome NOVA 2000e series volumetric gas adsorption instrument, which is a USA automated gas adsorption system using nitrogen as the adsorptive, is used for the BET-specific surface area and PSD measurement.
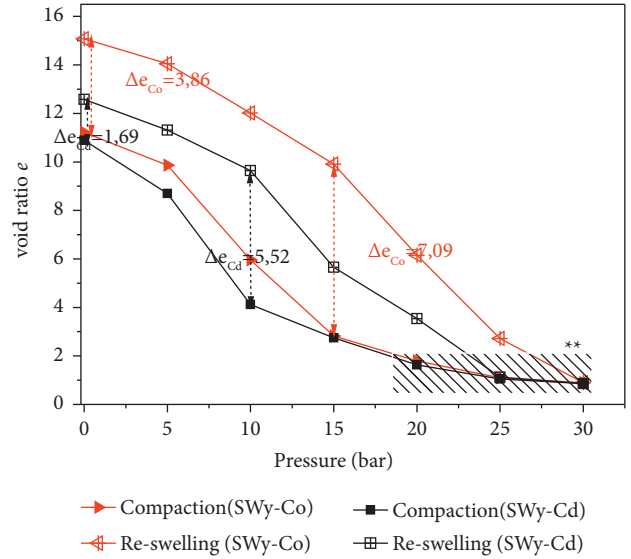

FIGURE 3: Equilibrium void ratio e for the compaction and reswelling versus applied pressure for SWy-Co and SWy-Cd samples. ∗∗ Zone of maximum applied pressure intensity.

Experience setting conditions are as follows: (i) adsorption isotherms are obtained at 77 K and at $P/P0 \sim 0.95$ (relative pressure); (ii) the SA and PSD measurements require the removal of adsorbed nitrogen and oxygen. This is carried out under reduced pressure (vacuum) at 100°C for 10 h. The desorption isotherms section, assuming a cylindrical pores model, is the basis of the application of the BJH method to define the PSD [82–91].

3. Results and Discussion

3.1. The Oedometric Test: Compaction and Reswelling. Several parameters control the clay material response to mechanical stress. Montmorillonite fractions are characterized by high porosity and a total volume which essentially depends on the water content, the water saturation, and the water retention mechanisms. Other intrinsic/multiscale parameters ranging from the geological genesis to the individual layer nanometric properties influence the possible deformations [92–95]. This work investigates the response of metal-exchanged montmorillonite specimens (i.e., exchangeable cations are Co^{2+} or Cd^{2+}) to uniaxial mechanical stress ensured by an oedometric test (loading/unloading). The applied stress is confirmed by investigating the void ratio e modification giving the applied pressure (Figure 3). The reswelling curve is obtained following a release of the applied pressure (Table 1). At first sight, the compaction/reswelling curves show the deformation irreversibility process and the nonlinear process, whatever the exchanged cation nature, which agrees with [72, 91] works. This behaviour finds an explanation in [64], which attributes the observed nonlinearity of the consolidation characteristics to the correlation between the consolidation stress (σ_v) and the void ratio (e).

The observed nonlinearity during the loading/unloading process concerns only a single stress cycle which resulted in remarkable fluctuations in the void ratio values. The

TABLE 1: Equilibrium void ratio e for the compaction and reswelling data for SWy-Co and SWy-Cd samples. Zero bar corresponds to "free" swelling.

Mechanical constraint	P (bar)	0	5	10	15	20	25	30
Compaction	SWy-Co	11.22	9.86	5.96	2.82	1.79	1.10	0.90
Reswelling	SWy-Co	15.08	14.05	12.02	9.91	6.15	2.72	0.90
Compaction	SWy-Cd	10.89	8.69	4.12	2.75	1.63	1.05	0.86
Reswelling	SWy-Cd	12.58	11.31	9.64	5.66	3.54	1.13	0.86

microobjective here is to create material fatigue to examine its hydric behaviour afterwards by varying %rh under a controlled atmosphere. For the two samples, a gap separating the void ratio values Δe in the absence of applied pressure (pressure = 0 bar) is partly explained by the coexistence of two possible scenarios, respectively, irreversible energy losses and interparticle friction, which is an intrinsic phenomenon in lamellar structures and which occurs during the progressive alignment of the particles/crystallites by increasing constraint strength [87, 88].

To understand the obtained void ratio values fluctuations during the reswelling process, the effective stress parameter, the swelling index (Cs), and the compression index (Cc) are introduced. Indeed, [64] uses the constant rate of strain CRS test as a crucial parameter to explore the unloading behaviour of clay minerals. For that, the pore water pressure excess during the unloading sequence is modelled by an assumption based on a cubic polynomial equation. Indeed, the Cc or Cs variations are very sensitive to the consolidation time (at constant load before the unloading) consideration. Along the compaction/reswelling sequence and the global pressure range (0 to 30 bar), in the case of the SWy-Co sample, $\Delta e_{Co} = 3.86$. This value decreases in the case of the SWy-Cd sample to $\Delta e_{Cd} = 1.69$.

On the other hand, a maximum gap is observed for an applied pressure of 15 bar and for which Δe jumps to 7.09 for Co^{2+}. For Cd^{2+} cation, the maximum Cs and Cc fluctuations are observed at 10 bar when Δe jumps to 5.52. For a maximum applied pressure intensity (zone $**$ on Figure 3) and whatever the nature of the exchangeable cation, a similar behaviour of Cs and Cc is observed during the loading sequence from 15 bar. During the unload sequence (reswelling) and from 30 bar applied pressure values, a divergence between the evolution of Cc and Cs is observed.

This noted disparity is explained by the process irreversibility at the nanoscopic scale, where the layer organization inside the crystallite depends essentially on the composition of the interlamellar space (IS). The intrinsic IS configurations are affected by the nature of the exchangeable cation, which afterwards will affect the layer stacking and the crystallite geometry. In fact, the diffuse ion layers around the particles lead to interparticle repulsion ascribed to the osmotic activity of the ions. The existing repulsion force decreases when increasing, respectively, the distance between clay particles, electrolyte concentration, and exchangeable cation valence. It should be noted that the obtained data for the "free" swelling state is realized when the sample is constrained only by the friction of the piston.
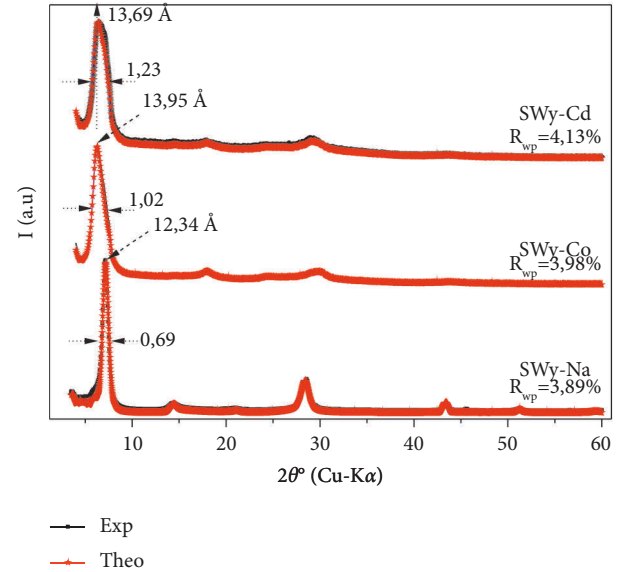

FIGURE 4: Best agreement obtained between theoretical (red scatter) and experimental (black line) profiles for all studied samples.

3.2. XRD Analysis of Unstressed Samples. The best agreement between the experimental and theoretical XRD profiles for the stressed samples is summarized in Figure 4. Qualitatively, a classical homogeneous 1 W layer phase is observed in the case of SWy-Na [67]. This hydration homogeneity is confirmed by the low values of FWHM and ξ parameter (Table 2) [74]. For the SWy-Co and SWy-Cd samples, an interstratified 1 W/2 W hydration character is observed throughout the entire exploited angular range. The initial d_{001} (Å) value increased (Table 2) towards 13.95 and 13.69, indicating probably the achievement of the cation exchange process and a new IS configuration. For both cases, the XRD profile geometry is characterized by an irrational 00l position (ξ parameter) with a large 001 refection (FWHM ($2\theta°$)) = 1.02 and 1.23). The 001 reflection is accompanied by a shoulder towards 7.48 ($2\theta°$) attributed to 1 W hydration phases ($d_{001} \approx 12$ Å). Generally, the observed asymmetric 001 reflection reflects the coexistence of several hydration states within the stack and/or an incomplete (partial) cation exchange. Two possible interpretations arise in this case. Either the cation exchange capacity (CEC) is fully saturated by the exchangeable cations, or a minor fraction of the starting Na^+ cation persists in the IS with partial cation exchange. Compared with the work of [58–60] and considering the ionic potential affinity of the two cations with optimized, verified, and reproducible experimental conditions,
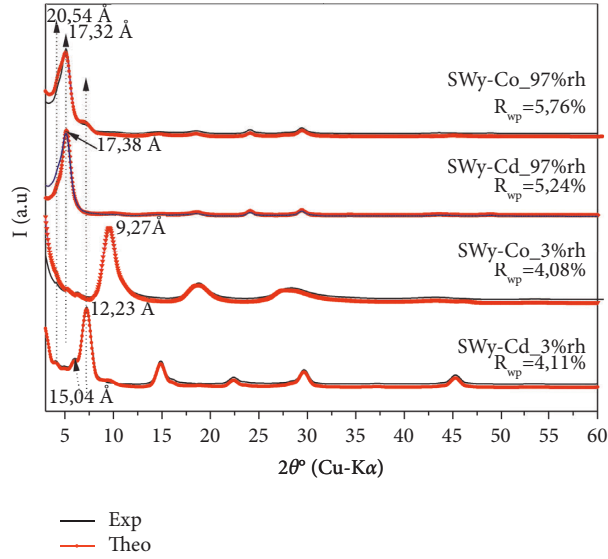
FIGURE 5: Best agreement obtained between theoretical and experimental profiles for stressed SWy-Cd and SWy-Co studied under extreme %rh value.

TABLE 2: Qualitative XRD investigation in the case of unstressed and stressed samples.

Samples	$2\theta°$	d_{001} (Å)	FWHM ($2\theta°$)	D (Å)	ξ (Å)	Hydration characters
Unstressed sample						
SWy-Na	7.16	12.34	0.69	25.13	0.086	Homogenous
SWy-Co	6.25	13.95	1.02	16.67	0.428	Interstratified
SWy-Cd	6.45	13.69	1.23	20.62	0.812	Interstratified
Stressed sample						
SWy-Co_3%rh	9.53	9.27	0.64	11.86	0.151	
SWy-Co_97%rh	5.10	17.32	1.41	10.67	0.875	Interstratified
	4.30	20.54				
SWy-Cd_3%rh	7.22	12.23	0.78	12.56	0.127	
	5.87	15.04				Interstratified
SWy-Cd_97%rh	5.08	17.38	1.33	11.14	0.788	
	4.39	20.11				

obtained results in the case of Cd^{2+} and Co^{2+} cation are in concordance. More details can be given later by quantitative XRD analysis. Quantitative XRD investigations are the solution to decide with the predictions of the qualitative analysis [70, 76]. Indeed, in the case of interstratified structures, several hypotheses are necessary, whose resolution requires a more in-depth theoretical approach. In the case of the SWy-Na sample, an agreement between the experimental and theoretical profile is obtained with an $R_{wp} = 3.89\%$ (Table 3). The position of the sodium and its hydration sphere at the medium of the IS respects the literature data [57]. On the other hand, the experimental profile is reproduced theoretically through a randomly distributed two phases, qualitatively inapparent, between a major contribution of the 1 W state (≈75%) and a minor contribution of (≈25%) relative to the 0 W layer.

The 00*l* reflections modelling approach in the case of the SWy-Co sample supposes the coexistence of three mixed layers structure MLS saturated with the Co^{2+} cation. Theoretical models exhibit variable hydration states (e.g., 1 W, 1 W/2 W, and 1 W/2 W). The used MLS (from the best

agreement) are decomposed into several layer populations (Table 3) assembled according to a specific succession probability law. The structural parameters released from theoretical models are summarized in Table 3. The MLS are obtained by weighted layer-type populations, which are expected to have, respectively, identical chemical composition, identical layer thickness, and identical Z coordinates of the atoms [67, 96–98].

The best fit of the experimental XRD pattern ($R_{wp} = 4.13\%$) (Figure 4) in the case of the SWy-Cd sample is obtained through theoretical models mainly composed of an interstratified structure using three MLSs including various relative proportions of the hydrated layer (Table 3). The foremost remark in this case is the presence of a reasonable 1 W phase weight (9.04%) attributable to the saturation of the material CEC by starting Na^+ cation. This agrees with the starting assumption concerning the observed experimental 001 reflection shoulder at 7.48 ($2\theta°$). This result calls into question the achievement of the cation exchange process despite compliance with the reproducibility of the experimental cation exchange protocol.

TABLE 3: Optimal structural parameters taken from quantitative XRD analysis for all studied samples.

Sample	%MLS	xW_Exc.Cat	L.Th (Å)	n_{H2O}	W_A	P_{AA}	M	M_{tot}	$\%R_{wp}$
SWy-Na	74.3	1W_Na	12.2	1.5	1	1	12	9	3.89
	25.7	0W_Na	12.2	0	1	1	5		
	52.36	1W_Co	12.2	0.8	1	1	11		
		1W_Na	12.2	0.4	0.7				
SWy-Co unstressed	33.84	2W_Co	15.2	0.3 / 0.3	0.3	0.59	7	9	3.98
		1W_Co	12.2	0.4	0.5				
	13.80	2W_Co	15.2	0.3 / 0.3	0.5	0.5	5		
	51.44	1W_Cd	12.2	0.9	1	1	12		
		1W_Cd	12.2	0.15	0.7				
SWy-Cd unstressed	39.52	2W_Cd	15.2	0.15 / 0.15	0.3	0.71	6	14	4.13
	9.04	1W_Na	10	1.5	1	1	6		
	68.61	0W_Co	9.5	0	1	1	12		
		0W_Co	9.5	0	0.7				
SWy-Co stressed 3%rh	31.39	0W_Na	9.3	0 / 0	0.3	0.72	5	10	4.08
	65.21	1W_Cd	12.2	0.7	1	1	12		
		1W_Cd	12.2	0.1	0.7				
SWy-Cd stressed 3%rh	31.52	1W_Na	12.3	0.1 / 0.1	0.3	0.6	5	10	4.11
	3.27	0W_Cd	9.8	0	1	1	4		
	70.20	3W_Co	18.1	1.5	1	1	8		
		3W_Na	18.2	1.5	0.7				
SWy-Co stressed 97%rh	23.50	4W_Co	21.1	2 / 2	0.3	0.7	5	7	5.76
	6.30	2W_Na	15.2	1	1	1	4		
		3W_Cd	18.2	1.5	0.3				
	70.47	4W_Cd	21.2	2.1 / 2.1	0.7	0.3	8	7	5.24
SWy-Cd stressed 97%rh		3W_Cd	18.2	1.5	0.7				
	27.57	2W_Na	15.2	1.2 / 1.2	0.3	0.7	5		
	1.96	2W_Na	10	1	1	1	5		

Note. xW_Exc.Cat: layer type and the associated exchangeable cation; L.Th: layer thickness in Å. 2 W, 1 W, and 0 W are attributed to the layer hydration state. n_{H2O}: the number of H_2O molecules per half unit cell. Z_{H2O}: position along $c*$ axis of H_2O molecule is fixed to 10.5 Å, 11.3 Å//13.6 Å, 11.3 Å//13.6 Å//16.6 Å, and 11.3 Å//13.6 Å/16.6 Å//19.3 Å, respectively, for 1 W, 2 W, 3 W, and 4 W hydration state. The position of exchangeable cations per half unit cell calculated along the c∗ axis is fixed to 8.6 Å, 10.50 Å, 12.4 Å, 14.7 Å, and 16.8 Å, respectively, for 0 W, 1 W, 2 W, 3 W, and 4 W hydration state [78]. $-n_{EXC.CAT}$: the number of exchangeable cations per half unit cell is fixed to 0.33 (for Na^+ cation) and 0.165 for (Co^{2+} and Cd^{2+} cation), indicating full saturation of the cation exchange capacity (CEC).

3.3. XRD Analysis of Mechanically Stressed Samples

3.3.1. Qualitative Investigation. The effect of the applied mechanical stress on the hydration properties of Cd^{2+} and Co^{2+} exchanged montmorillonite is addressed by varying the %rh rate under a controlled atmosphere. The goal is to see the structural evolution of the studied specimens under extreme %rh values (3%rh and 97%rh) (after environment equilibrium), which then allows us to simulate real IS changes affected using clay as a geological membrane. Experimental XRD patterns obtained in the case of SWy-Cd at 3%rh show a $d_{001} = 12.23$ Å indicating probably a 1 W hydration state. An interstratified hydration trend is confirmed by the elevated FWHM and ξ parameter value (Table 2). Indeed, a left-handed profile asymmetry towards the low angles ($2\theta = 5.84°$; $d_{001} = 15.04$ Å), which is ascribed to a minor 2 W hydration state phase, was observed despite the conditioned dry environment. The d_{001} basal spacing value shows conservation of the 1 W hydration state regardless of the experimental equilibrium achieved at 3%rh (one hour of equilibrium with its environment before starting the XRD recording).

For the SWy-Co at 3%rh, the sample seems more sensitive to the %rh level drop, and the $d_{001} = 9.27$ Å indicates a basically dehydrated 0 W state. The observed result is a real manifestation not only of the %rh fluctuations effect but also of the mechanical stress already applied through the compaction and reswelling cycle. The conclusion that can be drawn by qualitative comparison between these two samples (having undergone the same stresses) lies in the modification of the IS organization. Indeed, the basal spacing shift is directly related to the new IS organization, which is very

sensitive to the electrostatic and chemical bonding forces governing the IS equilibrium.

The IS water molecules insertion/release mechanism is interpreted by a hypothesis based on three freedom degree fluctuations, including, respectively, the positions, the abundances of the IS species, and the associated layer stacking probabilities. All cited structural parameters, treated individually or coupled, complicate and/or facilitate the water molecule release process, which can be established when decreasing the %rh rate. This hypothesis is since interpreted in the case of the SWy-Cd sample by the free water transformation (supporting cation exchange process) from the surrounding environment into structural water (intrinsic layer composition), incorporated in the internal and external pore surfaces, which complicates its loss by dehydration [60, 68]. It is noted that, in the case of the SWy-Co sample, an uncomplicated release of an IS water molecule is observed.

At 97%rh, SWy-Cd and SWy-Co are characterized by an asymmetric 00l reflection profile (Figure 5). Both samples present a high hydration state with d_{001} equal, respectively, to 17.38 Å and 17.32 Å, indicating probably a transition to the 3 W hydration state. A shoulder towards the small angles (d_{001} = 20.54 Å), which is attributed to a beginning 3 W⟶4 W hydrous transition state, is observed. An interstratified global character is confirmed by the high values of FWHM and the rationality parameter.

3.3.2. XRD Profile Modelling Approach.

The best agreement between theoretical and experimental XRD patterns obtained at a variable %rh rate is confirmed by an acceptable R_{wp} that did not exceed 5.71%. Optimum structural parameters used to imitate experimental XRD profile are reported in Table 3.

The theoretical IS water molecule distribution and the compensator cation position follow a discrete distribution consistent with [57, 67, 74] works. For each accepted theoretical model, several layer types with variable stacking modes are used to improve the agreement. The partial segregation (R1) is the main MLS distribution adopted for all studied samples. At 3%rh, the experimental profile of the SWy-Cd sample is reproduced by mixing three MLS mainly composed of a major 1 W layer fraction (saturated by Cd^{2+} cation). For the same sample, a minor proportion of the Na^+ saturated layer is used. Generally, the absence of a monohomogeneous 1 W phase at 3%rh and an R1 stacking mode type is the main conclusion. In the case of the SWy-Co sample, which presents a 0 W hydration state at 3%rh, the diffracted intensity is reproduced by two MLS (0 W) mainly saturated by Co^{2+} and Na^+ cations (Table 3). At 97%rh and regardless of the exchangeable cation nature, the 0 W and 1 W phase contribution in the MLS disappears. The experimental profiles are entirely reproduced by a three-MLS combination characterized by variable weighted layer population. For SWy-Co, a minority bihydrated phase related to Na^+ cation is introduced, and the major layer fraction saturated by Co^{2+} cation (extremely hydrated 3 W or 4 W water layers) is used to obtain a good fit.
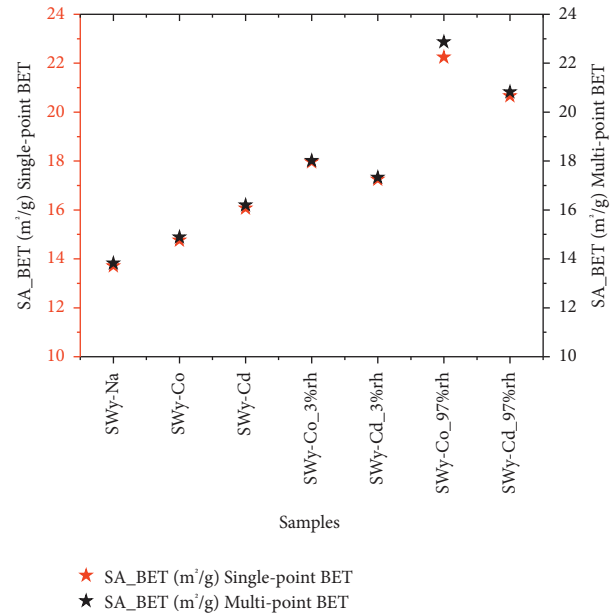

FIGURE 6: SA_{BET} single and multipoint BET for unstressed and stressed samples.

For SWy-Cd, the structure is completely matched by combining three MLS. Indeed, theoretical models contain a major contribution of 3 W/4 W phase, and the sample retains its interstratified character, which is in accordance with the qualitative description mentioning an interstratified phase. Among the strengths of the modelling approach, the accurate structural heterogeneities identification is related to the coexistence of variable layer populations within the clay particle. Subsequently, it allows us to show the structural changes affecting the IS after applying stresses (Table 3).

3.4. Adsorption and Porosity Features.

The clay properties are mainly monitored by their internal and external surface. The total surface includes the external surface, between the clay particles, and the inner surface, relating to the IS. Internal and external layer surfaces are affected during the compaction and reswelling process. The surface modification will probably influence the chemical and physical bonds with the IS content and the adsorption properties. The layer stacking distribution is affected by the applied mechanical constraint (results obtained from XRD analysis), and a possible consequent porosity disturbance may be conducted. In fact, after stress release, the configuration theoretically leans towards a new equilibrium, which differs from the starting configuration [99, 100].

The montmorillonite porosity is still poorly characterized because of the difficulty of visualizing hydrated samples in their original condition. The potential relation between porosity, CEC, crystallite shape/size, and applied mechanical stress is assured by the correlation of BET adsorption measurement and BJH pore size distribution analysis. Single-point and multipoint BET methods (based on the surface area (SA)) are used to assess the possible chemical transformation affecting the external clay layer surface. This

purpose is achieved from nitrogen isotherms [90]. To measure the average pore diameter for each sample, a BJH method is applied. The obtained results from adsorption measurement and porosity for all studied samples are summarized in Figures 4 and 7. Results show an increase in the calculated external surface for samples having undergone mechanical stress, whatever the nature of the exchangeable cation and the constraint type (compaction or reswelling).

By comparing SA value evolution, after applying mechanical stress, a logical values boost is observed for the stressed samples, whatever the applied %rh rate. This is probably interpreted by a crystallite exfoliation tendency which results in a decrease in the average number of layers per crystallite following the layer cohesion damage. Also, it can be interpreted by the diffusion coefficient alteration in relation to the packaging density of the montmorillonite. For saturated CEC by Co^{2+} cations, high SA values are obtained, suggesting the effect of the exchangeable cation nature on the new IS configuration (Figure 6). The average nanopore diameter (Figure 7) respects the same trend with values boost after stress regardless of the cation exchanged.

For all examined samples, an isotherm of nitrogen adsorption- (ads-) desorption (des) was presented (Figure 8). A type II adsorption isotherm [84, 86, 90] is closer to the shape of the obtained curves. This allocation is due to the mesoporous texture described by coexisting of large pores with nanopores, which agrees with the pore sizes distribution for the porous materials. Large pore sizes obtained in the case of stressed SWy-Co sample are justified by the coupling of three essential parameters, respectively, the loading/ unloading cycle, the %rh fluctuations (which constitutes a hydrous constraint), and the nature of the exchangeable cation. The Co^{2+} ions exchange promotes the exfoliation process and thereafter increases the porosity degree.

The SA concept does not permit a full textural description extending from 2D to 3D in the case of lamellar structures. The failures and limitations of SA results interpretation involve improvements established on the PSD analysis to access IS information. The PSD analysis is directed based on several approximations summarized in Table 4. The V-r (cumulative pore volume versus pore radius) plots or the mesopore PSD are given in Figure 9. A considerable disparity between SWy-Co and SWy-Cd sample pore size evolution was obtained. For unstressed and stressed samples, the saturated SWy-Co specimen varies in a very close way to the SWy-Cd sample, provided that the diameter of the pores does not exceed 3 nm. For higher values, a divergence appears with a "gap" in favor of Co^{2+} cation, which reaches 0.0068 mL/g (Figure 9). The obtained V-r variation proves, initially, the achievement of the cation exchange process, which is confirmed by specific V-r curve trends yet showing the same appearance. In addition, an increase in the V-r "gap" for stressed samples seems like the direct effect of the application of mechanical stresses. The V-r curve radius derivative for all samples is given in Figure 10.
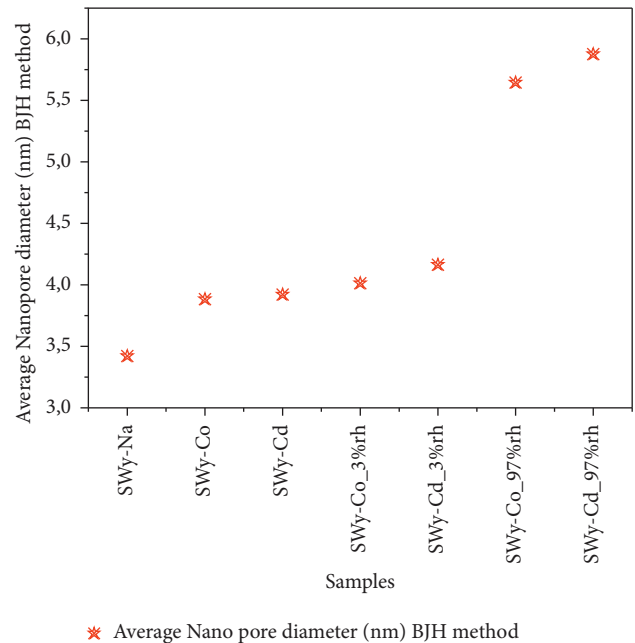

FIGURE 7: BJH method average pore diameter for unstressed and stressed samples.

The maximum mesopore volume (0.00620 mL/g) reached at 3.99 nm is obtained for the stressed SWy-Co sample. In this case, the determined V-r values are far greater than those relating to SWy-Cd. The gap between the two stressed samples exaggerates until it reaches gap values of 0.0030. This variation is consistent with the XRD modelling profile, which predicts layer exfoliation and presence of a highly hydrated rate (4 W) for both SWy-Co and SWy-Cd. Commonly, the applied mechanical stress affected the volume of the mesopores, which are in any case greater than those determined for the starting sample. For all samples, the mesopore radii varied between 1.598 and 16.828 nm (Figure 10). The porosity investigation using the BET-BJH method confirms obtained results from XRD modelling approach indicating, respectively, high hydration rate layer exfoliation trends and crystallite size fluctuations induced by stress.

The maximum mesopore volume (0.00620 mL/g) is obtained for the stressed SWy-Co sample. The determined V-r values, in the case of SWy-Co, are far greater than those relating to SWy-Cd. For the stressed SWy-Co sample, the maximum mesopore volume is 0.00620 mL/g and obtained at 3.99 nm. The gap between the two stressed samples exaggerates until it reaches gap values of 0.0030. This variation is consistent with the XRD modelling profile, which predicts layer exfoliation and presence of a highly hydrated rate (4 W) for both SWy-Co and SWy-Cd. Commonly, the applied mechanical stress affected the volume of the mesopores, which are in any case greater than those determined for the starting sample. For all samples, the mesopore radii varied between 1.598 and 16.828 nm (Figure 10). The porosity investigation using the BET-BJH method confirms
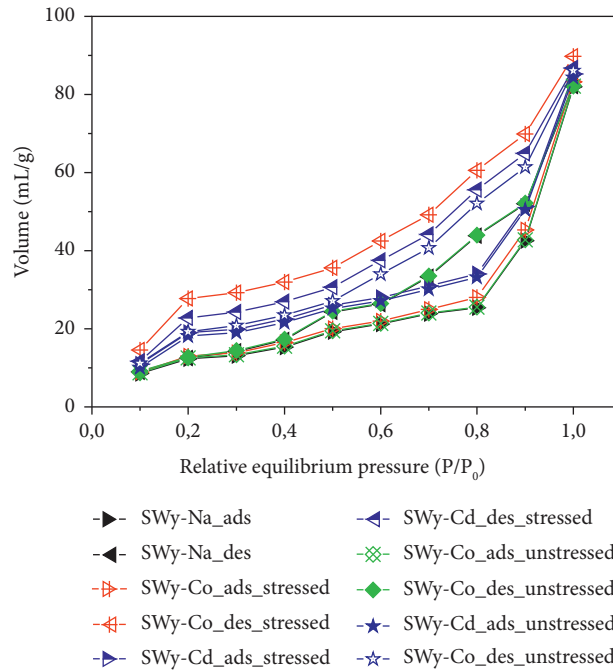
FIGURE 8: Nitrogen adsorption- (ads-) desorption (des) isotherms.

TABLE 4: The basic physical approximations adopted for the PSD analysis.

| Technical side	Fundamental side
P_0 is the vapor pressure of the bulk liquid nitrogen at the liquid nitrogen temperature (~ 77 K)	Cylindrical pores shape
P is the equilibrium pressure of desorption at the liquid nitrogen temperature (~ 77 K)	Cylindrical pores radius (r) approximatively half of its width
The volumes of micropores, mesopores, and macropores, including nanopores in one gram solid, are labelled, respectively, V_{Mi}, V_{Me}, and V_{Ma} (all in mL/g)	Cylindrical mesopores with radii (r) corresponding to V values calculated from the corrected Kelvin equation using P/P_0 values
Specific micromesopore volumes ($V = V_{Mi} + V_{Me}$) is determined using the desorption data (at the relative equilibrium pressure P/P_0)	Macropores do not affect the adsorptive properties [76]
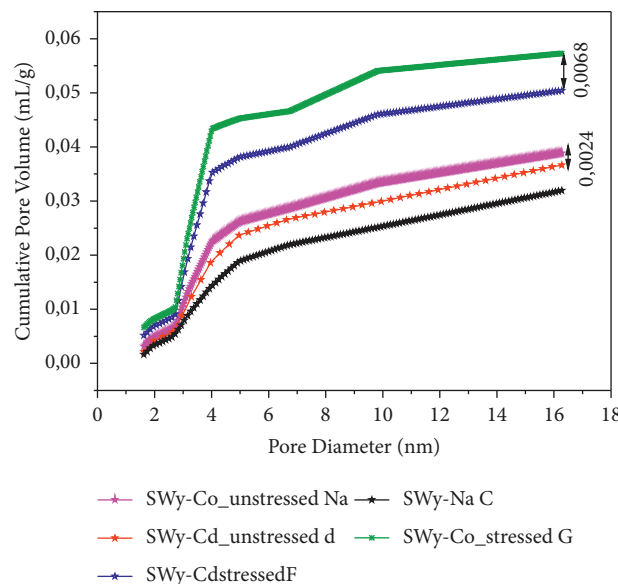
FIGURE 9: The pore size distribution (PSD) curve for the different studied samples (V-r).
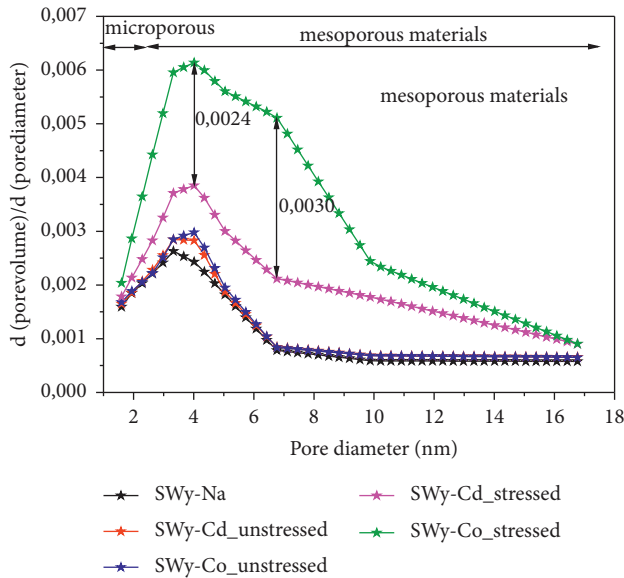
FIGURE 10: The derivative pore size distribution curve.

obtained results from XRD modelling approach indicating, respectively, high hydration rate layer exfoliation trends and crystallite size fluctuations after stress.

4. Conclusion

This work investigates structural impact, IS response, quantitative CEC instabilities, and porosity alteration of metal-exchanged montmorillonite (Co^{2+} and Cd^{2+}) according to the mechanical constraints created at the laboratory scale. Structures heterogeneities, hydration behaviour, and relationships between macroscopic stresses and microscopic hydration properties have been disclosed through the XRD profile modelling approach and the adsorption measurement. Obtained results demonstrate the following: (i) The void ratio e deviation increases along the compaction/reswelling process regardless of the exchangeable cation nature. (ii) At a low extreme %rh rate (3%), a clear and easy 0 W dehydration process is observed for the Co^{2+} cation, which is not obvious for the Cd^{2+} cation, which keeps a 1 W hydration state despite the mechanical disturbance. (iii) A highly 3 W/4 W hydrated state appears for the two studied samples brought to 97%rh, which is explained by a reduction in the average number of layers per crystallite evidence of an exfoliation tendency and the ease of filling of the IS. (iv) At 97%rh, mechanical damage induces, respectively, a clear interstratified character, segregation layer stacking trends, sensitive layer-type junction probabilities, and an increase in the used MLS. (v) The adsorption measurement results confirm the exfoliation layer trends for stressed samples. (vi) The divergence of V-r fluctuations proves the achievement of the cation exchange process, which is confirmed by the specific conduct of the V-r curves despite having the same appearance. (vii) The mechanical stress effect is reflected in the V-r curve by a high "gap" for the stressed samples. (viii) The mesopore V-r shows raised values in the case of Co^{2+}

cation, indicating a new IS arrangement (compared with the starting sample) allowing better water profit for the SWy-Co sample [101–103].

Data Availability

The generated and analysed data during the current study are included within the article and can be obtained from the corresponding authors upon reasonable request.

Conflicts of Interest

The authors declare no conflicts of interest.

Authors' Contributions

Walid Oueslati (WO) was responsible for conceptualization, methodology, investigation, validation, formal analysis, visualization, data curation, resources, supervision, writing, editing, reviewing, and project administration. Chadha Mejri (CM) was responsible for investigation, visualization, and resources. Abdesslem Ben Haj Amara (ABHA) was responsible for methodology and resources.

Acknowledgments

The authors acknowledge the assistance provided by the editor.

References

[1] M. Tondel and L. Lindahl, "Intergenerational ethical issues and communication related to high-level nuclear waste repositories," *Current Environmental Health Reports*, vol. 6, no. 4, pp. 338–343, 2019.

[2] S. S. K. AB, "Long-term Safety for the Final Repository for Spent Nuclear Fuel at Forsmark," *Main Report Of the SR-Site Project*, vol. 1, p. 276, 2018.

[3] SELROOS, Jan-Olof et FOLLIN, Sven, "Overview of hydrogeological site-descriptive modeling conducted for the proposed high-level nuclear waste repository site at Forsmark, Sweden," *Hydrogeology Journal*, vol. 22, no. 2, pp. 295–298, 2014.

[4] G. Bernd, "Geological disposal of radioactive waste in clay," *Elements*, vol. 12, no. 4, pp. 239–245, 2016.

[5] R. C. Ewing, "Long-term storage of spent nuclear fuel," *Nature Materials*, vol. 14, no. 3, pp. 252–257, 2015.

[6] P. Landais, "Advances in geochemical research for the underground disposal of high-level, long-lived radioactive waste in a clay formation," *Journal of Geochemical Exploration*, vol. 88, no. 1-3, pp. 32–36, 2006.

[7] T. Manzel, C. Podlech, G. Grathoff, S. Kaufhold, and L.. N. Warr, "In situ measurements of the hydration behavior of compacted Milos (SD80) bentonite by wet-cell X-ray diffraction in an Opalinus clay pore water and a diluted cap rock brine," *Minerals*, vol. 11, no. 10, pp. 1082–1116, 2021.

[8] F. Claret, N. Marty, and C. Tournassat, "Modeling the long-term stability of multi-barrier systems for nuclear waste disposal in geological clay formations," in *Reactive Transport Modeling: Applications in Subsurface Energy, and Environmental Problems*, John Wiley and Sons, Eds., vol. 2018pp. 395–451, Chichester, UK, 2018.

[9] G. Montes-H, B. Fritz, A. Clement, and N. Michau, "Modeling of transport and reaction in an engineered barrier for radioactive waste confinement," *Applied Clay Science*, vol. 29, no. 3-4, pp. 155–171, 2005.

[10] S. Kaufhold and R. Dohrmann, "Distinguishing between more and less suitable bentonites for storage of high-level radioactive waste," *Clay Minerals*, vol. 51, no. 2, pp. 289–302, 2016.

[11] S. Norris, "Multiple roles of clays in radioactive waste confinement–introduction," *Geological Society, London, Special Publications*, vol. 482, no. 1, pp. 1–9, 2019.

[12] Y. Wang, "Leachate Management in the Aftercare Period of Municipal Waste Landfills," *Ph.D. Thesis*, Aalto University, Espoo, Finland, 2013.

[13] Z. Cooper, R. Bringolf, R. Cooper, K. Loftis, A. L. Bryan, and J. A. Martin, "Heavy metal bioaccumulation in two passerines with differing migration strategies," *Science of the Total Environment*, vol. 592, pp. 25–32, 2017.

[14] M. K. Widomski, W. Sțepniewski, and A. Musz-Pomorska, "Clays of different plasticity as materials for landfill liners in RuralSystems of sustainable waste management," *Sustainability*, vol. 10, no. 7, pp. 2489–2505, 2018.

[15] G. Xiao, G. Xu, T Wei, J Zeng, W Liu, and L Zhang, "The effect of Cu (II) on swelling and shrinkage characteristics of sodium bentonite in landfills," *Applied Sciences*, vol. 11, no. 9, pp. 3881–3894, 2021.

[16] P. C. Gomes, M. P. Fontes, A. G. da Silva, E. de S Mendonça, and A. R. Netto, "Selectivity sequence and competitive adsorption of heavy metals by Brazilian soils," *Soil Science Society of America Journal*, vol. 65, no. 4, pp. 1115–1121, 2001.

[17] A. Gupta, R. Zhao, J. T. Novak, and C. D. Goldsmith, "Variation in organic matter characteristics of landfill leachates in different stabilisation stages," *Waste Management & Research: The Journal for a Sustainable Circular Economy*, vol. 32, no. 12, pp. 1192–1199, 2014.

[18] S. Tahervand and M. Jalali, "Sorption and desorption of potentially toxic metals (Cd, Cu, Ni and Zn) by soil amended with bentonite, calcite and zeolite as a function of pH," *Journal of Geochemical Exploration*, vol. 181, pp. 148–159, 2017.

[19] W. Hu, S. Lu, W. Song et al., "Competitive adsorption of U (VI) and Co (II) on montmorillonite: a batch and spectroscopic approach," *Applied Clay Science*, vol. 157, pp. 121–129, 2018.

[20] M. Slaný, L. Jankovič, and J. Madejová, "Structural characterization of organo-montmorillonites prepared from a series of primary alkylamines salts: mid-IR and near-IR study," *Applied Clay Science*, vol. 176, pp. 11–20, 2019.

[21] G. Xiang, W. Ye, F. Yu, Y. Wang, and Y. Fang, "Surface fractal dimension of bentonite affected by long-term corrosion in alkaline solution," *Applied Clay Science*, vol. 175, pp. 94–101, 2019.

[22] H. Lakshmikantha and P. V. Sivapullaiah, "Geotechnical properties of cement treated illite as hydraulic barrier," *Clay Research*, vol. 22, no. 1-2, pp. 29–40, 2004.

[23] J. Bors, S. Dultz, and B. Riebe, "Retention of radionuclides by organophilic bentonite," *Engineering Geology*, vol. 54, no. 1-2, pp. 195–206, 1999.

[24] B Herlin and K. von Maubeuge, "Geosynthetic clay liners (GCLs)," in *Proceedings of the 4th International Pipeline Conference*, vol. 36207, pp. 211–216, 2002.

[25] M. Segad, S. Hanski, U. Olsson, J. Ruokolainen, T. Åkesson, and B. Jönsson, "Microstructural and swelling properties of Ca and Na montmorillonite: (in situ) observations with Cryo-TEM and SAXS," *Journal of Physical Chemistry C*, vol. 116, no. 13, pp. 7596–7601, 2012.

[26] W. Birmili, A. Charron, and R. Harrison, "Treatment of textile wastewater using bentonite clay as a natural coagulant," *Pediatric Transplantation*, vol. 11, pp. 895–900, 2014.

[27] H. Y. Shan and Y. J. Lai, "Effect of hydrating liquid on the hydraulic properties of geosynthetic clay liners," *Geotextiles and Geomembranes*, vol. 20, no. 1, pp. 19–38, 2002.

[28] S. Rosin-Paumier and N. Touze-Foltz, "Hydraulic and chemical evolution of GCLs during filter press and oedopermeametric tests performed with real leachate," *Geotextiles and Geomembranes*, vol. 33, pp. 15–24, 2012.

[29] B. Wang, J. Xu, B. Chen, X. Dong, and T. Dou, "Hydraulic conductivity of geosynthetic clay liners to inorganic waste leachate," *Applied Clay Science*, vol. 168, pp. 244–248, 2019.

[30] F. N. Charkley, K. Zhang, and G. Mei, "Shear strength of compacted clays as affected by mineral content and wet-dry cycles," *Advances in Civil Engineering*, vol. 2019, pp. 1–8, Article ID 8217029, 2019.

[31] U. Khalid, Z.. u. Rehman, C. Liao, K. Farooq, and H Mujtaba, "Compressibility of compacted clays mixed with a wide range of bentonite for engineered barriers," *Arabian Journal for Science and Engineering*, vol. 44, no. 5, pp. 5027–5042, 2019.

[32] A. Kaya and S. Durukan, "Utilization of bentonite-embedded zeolite as clay liner," *Applied Clay Science*, vol. 25, no. 1-2, pp. 83–91, 2004.

[33] M. Plötze, G. Kahr, R. Dohrmann, and H. Weber, "Hydromechanical, geochemical and mineralogical characteristics of the bentonite buffer in a heater experiment: The HE-B project at the Mont Terri Rock Laboratory," *Physics and Chemistry of the Earth, Parts A/B/C*, vol. 32, no. 8-14, pp. 730–740, 2007.

[34] S. M. Rao and T. Thyagaraj, "Swell–compression behaviour of compacted clays under chemical gradients," *Canadian Geotechnical Journal*, vol. 44, no. 5, pp. 520–532, 2007.

[35] M. Ammar and W. Oueslati, "Crystalline swelling process of Mg-exchanged montmorillonite: effect of external environmental solicitation," *Advances in Civil Engineering*, vol. 2018, pp. 1–18, Article ID 8130932, 2018.

[36] W. Oueslati, "Effect of soil solution pH during the tetracycline intercalation on the structural properties of a dioctahedral smectite: microstructural analysis," *Journal of Nanomaterials*, vol. 201917 pages, Article ID 7414039, 2019.

[37] M. K. Widomski, W. Stępniewski, and A. Musz-Pomorska, "Clays of different plasticity as materials for landfill liners in rural systems of sustainable waste management," *Sustainability*, vol. 10, no. 7, p. 2489, 2018.

[38] Z. Hu, K. Peng, L. Li et al., "Effect of wetting-drying cycles on mechanical behaviour and electrical resistivity of unsaturated subgrade soil," *Advances in Civil Engineering*, vol. 2019, pp. 1–10, Article ID 3465327, 2019.

[39] M. M.. A. Hussein, "Effect of sand compaction piles on the swelling and shrinkage behavior of expansive soil," *Advances in Civil Engineering*, vol. 202110 pages, Article ID 5582197, 2021.

[40] J. Lin, W. Zou, Z. Han, Z. Zhang, and X Wang, "Structural, volumetric and water retention behaviors of a compacted clay upon saline intrusion and freeze-thaw cycles," *Journal of Rock Mechanics and Geotechnical Engineering*, vol. 14, no. 3, pp. 953–966, 2022.

[41] R. Pusch, S. Knutsson, L. Al-Taie, and M. H. Mohammed, "Optimal ways of disposal of highly radioactive waste," *Natural Science*, vol. 04, no. 11, pp. 906–918, 2012.

[42] N. P. Laverov, S. V. Yudintsev, B. T. Kochkin, and V. I. Malkovsky, "The Russian strategy of using crystalline rock as a repository for nuclear waste," *Elements*, vol. 12, no. 4, pp. 253–256, 2016.

[43] Hennig, Theresa, and Michael KÜhn, "Potential Uranium Migration within the Geochemical Gradient of the Opalinus Clay System at the Mont Terri," *Minerals*, vol. 11, no. 10, p. 1087, 2021.

[44] M. Birgersson, O. Karnland, and U. Nilsson, "Freezing in saturated bentonite A thermodynamic approach," *Physics and Chemistry of the Earth, Parts A/B/C*, vol. 33, pp. S527–S530, 2008.

[45] S. D. Baxter, D. Holton, S. Williams, and S. Thompson, "Predictions of the wetting of bentonite emplaced in a crystalline rock based on generic site characterization data," *Geological Society, London, Special Publications*, vol. 482, no. 1, pp. 285–300, 2019.

[46] T. Ishii, M. Kawakubo, H. Asano et al., "A resistivity-based approach to determining the rates of groundwater seepage into buffer materials," in *Geological Society, London, Special Publications*, S Norris, E.A.C. Neeft, and M Van Geet, Eds., vol. 482, no. 1, pp. 205–212, 2019.

[47] E. E. Dagher, T. S. Nguyen, and J. A. Infante Sedano, "Development of a mathematical model for gas migration (two-phase flow) in natural and engineered barriers for radioactive waste disposal," *Geological Society, London, Special Publications*, vol. 482, no. 1, pp. 115–148, 2019.

[48] S. Finsterle, B. Lanyon, M. Åkesson et al., "Conceptual uncertainties in modelling the interaction between engineered and natural barriers of nuclear waste repositories in crystalline rocks," *Geological Society, London, Special Publications*, vol. 482, no. 1, pp. 261–283, 2019.

[49] V. I. Malkovsky, Y. P. Dikov, E. E. Asadulin, and V. V. Krupskaya, "Influence of host rocks on composition of colloid particles in groundwater at the Karachai Lake site," *Clay Minerals*, vol. 47, no. 3, pp. 391–400, 2012.

[50] P. Sellin and O. X. Leupin, "The use of clay as an engineered barrier in radioactive-waste management—a review," *Clays and Clay Minerals*, vol. 61, no. 6, pp. 477–498, 2013.

[51] M. Ammar, W. Oueslati, H. Ben Rhaiem, and A. Ben Haj Amara, "Effect of the hydration sequence orientation on the structural properties of Hg exchanged montmorillonite: quantitative XRD analysis," *Journal of Environmental Chemical Engineering*, vol. 2, no. 3, pp. 1604–1611, 2014.

[52] R. Chalghaf, W. Oueslati, M. Ammar, H.. B. Rhaiem, and A. B.. H. Amara, "Effect of an in situ hydrous strain on the ionic exchange process of dioctahedral smectite: case of solution containing (Cu^{2+}, Co^{2+}) cations," *Applied Surface Science*, vol. 258, no. 22, pp. 9032–9040, 2012.

[53] R. Chalghaf, W. Oueslati, M. Ammar, H.. B. Rhaiem, and ABH Amara, "Effect of temperature and pH value on cation exchange performance of a natural clay for selective (Cu^{2+}, Co^{2+}) removal: Equilibrium sorption and kinetics," *Progress in Natural Science*, vol. 23, no. 1, pp. 23–35, 2013.

[54] P. Delage, Y. J. Cui, and A. M. Tang, "Clays in radioactive waste disposal," *Journal of Rock Mechanics and Geotechnical Engineering*, vol. 2, no. 2, pp. 111–123, 2010.

[55] G. Xiang, W. Ye, Y. Xu, and F. E. Jalal, "Swelling deformation of Na-bentonite in solutions containing different cations," *Engineering Geology*, vol. 277, Article ID 105757, 2020.

[56] N. Güven and S. W. Bailey, "Hydrous Phyllosilicates (exclusive of micas)," *Reviews in Mineralogy*, vol. 19, p. 497, 1988.

[57] T. Sato, T. Watanabe, and R. Otsuka, "Effects of layer charge, charge location, and energy change on expansion properties of dioctahedral smectites," *Clays and Clay Minerals*, vol. 40, no. 1, pp. 103–113, 1992.

[58] I. Bérend, J. M. Cases, M. François et al., "Mechanism of adsorption and desorption of water vapour by homoionic montmorillonites: 2. the Li^+, Na^+, K^+, Rb^+ and Cs^+ exchanged forms," *Clays and Clay Minerals*, vol. 43, no. 3, pp. 324–336, 1995.

[59] J. M. Cases, I. Bérend, M. François, J. P. Uriot, L. J. Michot, and F. Thomas, "Mechanism of adsorption and desorption of water vapour by homoionic montmorillonite: 3. The Mg^{2+}, Ca^{2+}, Sr^{2+} and Ba^{2+} exchanged forms," *Clays and Clay Minerals*, vol. 45, no. 1, pp. 8–22, 1997.

[60] W. Oueslati, H. Ben Rhaiem, and A. Ben Haj Amara, "Effect of relative humidity constraint on the metal exchanged montmorillonite performance: an XRD profile modeling approach," *Applied Surface Science*, vol. 261, pp. 396–404, 2012.

[61] W. F. Moll, "Baseline studies of the Clay Minerals Society Source Clays: Geological Origin," *Clays And Clay Minerals*, vol. 49, no. 5, pp. 374–380, 2001.

[62] A. R. Mermut and A. F. Cano, "Baseline studies of the clay minerals society Source clays: chemical analyses of major elements," *Clays and Clay Minerals*, vol. 49, no. 5, pp. 381–386, 2001.

[63] H. Heller and R. Keren, "Rheology of Na-rich montmorillonite suspension as affected by electrolyte concentration and shear rate," *Clays and Clay Minerals*, vol. 49, no. 4, pp. 286–291, 2001.

[64] H. Tanaka, D. R. Shiwakoti, O. Mishima, Y. Watabe, and M. Tanaka, "Comparison of mechanical behavior of two overconsolidated clays: yamashita and Louiseville clays," *Soils and Foundations*, vol. 41, no. 4, pp. 73–87, 2001.

[65] H. Tanaka, A. Tsutsumi, and T. Ohashi, "Unloading behavior of clays measured by CRS test," *Soils and Foundations*, vol. 54, no. 2, pp. 81–93, 2014.

[66] A. Altomare, N. Corriero, C. Cuocci, A. Falcicchio, A. Moliterni, and R. Rizzi, "QUALX2.0: a qualitative phase analysis software using the freely available database POW_COD," *Journal of Applied Crystallography*, vol. 48, no. 2, pp. 598–603, 2015.

[67] W. Oueslati and M. Meftah, "Discretization of the water uptake process of Na-montmorillonite undergoing atmospheric stress: XRD modeling approach," *Advances in Materials Science and Engineering*, vol. 117 pages, Article ID 5219624, 2018.

[68] M. Ammar, W. Oueslati, N. Chorfi, and A. B.. H. Amara, "The water retention mechanism of a Cs^+ and Na^+ exchanged montmorillonite: effect of relative humidity and ionic radius on the interlayer," *Powder Diffraction*, vol. 30, no. S1, pp. S70–S75, 2015.

[69] W. Oueslati, H. B Rhaiem, and A. B. H Amara, "XRD investigations of hydrated homoionic montmorillonite saturated by several heavy metal cations," *Desalination*, vol. 271, no. 1-3, pp. 139–149, 2011.

[70] B. Lanson, "Modelling of X-ray diffraction profiles: investigation of defective lamellar structure crystal chemistry," *EMU Notes Mineral*, vol. 11, pp. 151–202, 2011.

[71] V. A. Drits, C. Tchoubar, and P. Klimanek, "X ray diffraction by disordered lamellar structures," *Theory and Applications to Microdivided Silicates and Carbons*, Springer-Verlag, 1991.

[72] W. Oueslati, N. Chorfi, and M. Abdelwahed, "Effect of mechanical constraint on the hydration properties of Na-montmorillonite: study under extreme relative humidity conditions," *Powder Diffraction*, vol. 32, no. S1, pp. S160–S167, 2017.

[73] B. A. Sakharov and B. Lanson, "X-ray identification of mixed-layer structures: modelling of diffraction effects," *Developments in Clay Science*, vol. 5, pp. 51–135, 2013.

[74] E. Ferrage, B. Lanson, N. Malikova, A. Plancon, B. A. Sakharov, and V. A. Drits, "New insights on the distribution of interlayer water in Bi-hydrated smectite from X-ray diffraction profile modeling of 00l reflections," *Chemistry of Materials*, vol. 17, no. 13, pp. 3499–3512, 2005.

[75] E. Ferrage, B. Lanson, B. A. Sakharov, N. Geoffroy, E. Jacquot, and V. A. Drits, "Investigation of dioctahedral smectite hydration properties by modeling of X-ray diffraction profiles: influence of layer charge and charge location," *American Mineralogist*, vol. 92, no. 10, pp. 1731–1743, 2007.

[76] M. Ammar, W. Oueslati, H. Ben Rhaiem, and A. Ben Haj Amara, "XRD profile modeling approach tools to investigate the effect of charge location on hydration behavior in the case of metal exchanged smectite," *Powder Diffraction*, vol. 28, no. S2, pp. S284–S300, 2013.

[77] C. Mejri, W. Oueslati, and A. B. H Amara, "How the solid/liquid ratio affects the cation exchange process and porosity in the case of dioctahedral smectite: structural analysis?" *Adsorption Science and Technology*, vol. 2021, pp. 1–24, Article ID 9732092, 2021.

[78] B. A. Sakharov, A. S. Naumov, and V. A. Drits, "X-ray diffraction by mixed-layer structures with a random distribution of stacking faults," *Soviet Physics - Doklady*, vol. 27, p. 523, 1982.

[79] B. A. Sakharov, H. Lindgreen, and V. A. Drits, "Mixed-layer kaolinite-illite-vermiculite in north sea shales," *Clay Minerals*, vol. 34, no. 2, pp. 333–344, 1999.

[80] Z. Sun, Y. G Chen, and W. M Ye, "Adsorption of Eu (III) onto Gaomiaozi bentonite corroded by cement waters: effect of cement solutions on the long-term sorption performance of bentonite in the repository conditions," *Journal of Cleaner Production*, vol. 251, Article ID 119692, 2020.

[81] M. Benzina and A. Bellagi, "Détermination des propriétés du réseau poreux de matériaux argileux par les techniques d'adsorption d'azote et de porosimétrie au mercure en vue de leur utilisation pour la récupération des gaz," *Annales de Chimie*, vol. 15, no. 6, pp. 315–335, 1990.

[82] S. J. Gregg, K. S. W. Sing, and H. W. Salzberg, "Adsorption surface area and porosity," *Journal of the Electrochemical Society*, vol. 114, no. 11, p. 279Ca, 1967.

[83] L. Yu, W. L. Hsu, J. A. Shamim, and H. Daiguji, "Pore network modeling of a solid desiccant for dehumidification applications," *International Journal of Heat and Mass Transfer*, vol. 186, Article ID 122456, 2022.

[84] P. Pang, H. Han, L. Hu, C. Guo, Y. Gao, and Y. Xie, "The calculations of pore structure parameters from gas adsorption experiments of shales: which models are better?" *Journal of Natural Gas Science and Engineering*, vol. 94, Article ID 104060, 2021.

[85] J. C. Groen, L. A. Peffer, and J. Pérez-Ramírez, "Pore size determination in modified micro- and mesoporous materials. Pitfalls and limitations in gas adsorption data analysis," *Microporous and Mesoporous Materials*, vol. 60, no. 1-3, pp. 1–17, 2003.

[86] E. P. Barrett, L. G. Joyner, and P. P. Halenda, "The determination of pore volume and area distributions in porous substances. I. Computations from nitrogen isotherms," *Journal of the American Chemical Society*, vol. 73, no. 1, pp. 373–380, 1951.

[87] T. Liu, L. Ju, Y. Zhou et al., "Effect of pore size distribution (PSD) of Ni-Mo/Al_2O_3 catalysts on the Saudi Arabia vacuum residuum hydrodemetallization (HDM)," *Catalysis Today*, vol. 271, pp. 179–187, 2016.

[88] K. Sing, "The use of nitrogen adsorption for the characterisation of porous materials," *Colloids and Surfaces A: Physicochemical and Engineering Aspects*, vol. 187, pp. 3–9, 2001.

[89] P. Kumar, R. V. Jasra, and T. S. G. Bhat, "Evolution of porosity and surface acidity in montmorillonite clay on acid activation," *Industrial & Engineering Chemistry Research*, vol. 34, no. 4, pp. 1440–1448, 1995.

[90] J. M. Zielinski and L. Kettle, *Physical Characterization: Surface Area and Porosity*, Intertek, London, 2013.

[91] H. Ben Rhaiem, C. H. Pons, and D. Tessier, "Factors affecting the microstructure of smectites. Role of cation and history of applied stresses," *The Clay Minerals Society, Bloomington IN*, vol. 1985, pp. 292–297, 1985.

[92] G. Q. Cai, C. G. Zhao, J. Li, and Y. Liu, "A new triaxial apparatus for testing soil water retention curves of unsaturated soils under different temperatures," *Journal of Zhejiang University - Science*, vol. 15, no. 5, pp. 364–373, 2014.

[93] C. F. Chiu and C. W. Ng, "Coupled water retention and shrinkage properties of a compacted silt under isotropic and deviatoric stress paths," *Canadian Geotechnical Journal*, vol. 49, no. 8, pp. 928–938, 2012.

[94] J. H. Atkinson and P. L. Bransby, *The Mechanics of Soils: An Introduction to Critical State Soil Mechanics*, McGraw-Hill, London, 1978.

[95] N. Saiyouri, D. Tessier, and P. Y. Hicher, "Experimental study of swelling in unsaturated compacted clays," *Clay Minerals*, vol. 39, no. 4, pp. 469–479, 2004.

[96] A. C. Inigo, D. Tessier, and M. Pernes, "Use of X-ray transmission diffractometry for the study of clayparticle orientation at different water contents," *Clays and Clay Minerals*, vol. 48, no. 6, pp. 682–692, 2000.

[97] B. Dazas, B. Lanson, A. Delville et al., "Influence of tetrahedral layer charge on the organization of interlayer water and ions in synthetic Na-saturated smectites," *Journal of Physical Chemistry C*, vol. 119, no. 8, pp. 4158–4172, 2015.

[98] F. Hubert, L. Caner, A. Meunier, and B. Lanson, "Advances in characterization of soil clay mineralogy using X-ray diffraction: from decomposition to profile fitting," *European Journal of Soil Science*, vol. 60, no. 6, pp. 1093–1105, 2009.

[99] S. Charpentier and G. Bourrié, "Deformation of saturated clays under mechanical and osmotic stress and its relation with the arrangement of the clays," *European Journal of Soil Science*, vol. 48, no. 1, pp. 49–57, 1997.

[100] G. R. Rao, I. Srikanth, and K. L. Reddy, "Effect of organo-modified montmorillonite nanoclay on mechanical, thermal and ablation behavior of carbon fiber/phenolic resin composites," *Defence Technology*, vol. 17, no. 3, pp. 812–820, 2021.

[101] K. Yotsuji, Y. Tachi, H. Sakuma, and K. Kawamura, "Effect of interlayer cations on montmorillonite swelling: comparison between molecular dynamic simulations and experiments," *Applied Clay Science*, vol. 204, Article ID 106034, 2021.

[102] G. Wang, L. Ran, J. Xu et al., "Technical development of characterization methods provides insights into clay mineral-water interactions: a comprehensive review," *Applied Clay Science*, vol. 206, Article ID 106088, 2021.

[103] A. Asaad, F. Hubert, E. Ferrage et al., "Role of interlayer porosity and particle organization in the diffusion of water in swelling clays," *Applied Clay Science*, vol. 207, Article ID 106089, 2021.